Treatment of Tricuspid Regurgitation at Subvalvular Level: Hemodynamic and Morphological Assessment in Ex-Vivo Beating Heart Model

Michal Jaworek, Omar A. Pappalardo, Matteo Selmi, Guido Gelpi, Claudia Romagnoni, Federico Lucherini, Nina Ajmone-Marsan, Alberto Redaelli, Gianfranco B. Fiore, Emiliano Votta, Carlo Antona & Riccardo Vismara
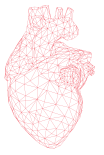
ORIGINAL RESEARCH

Check for updates

Treatment of Tricuspid Regurgitation at Subvalvular Level: Hemodynamic and Morphological Assessment in Ex-Vivo Beating Heart Model

Michal Jaworek, PhD [a,b], Omar A. Pappalardo, PhD [c], Matteo Selmi, PhD [d], Guido Gelpi, MD [b,e],
Claudia Romagnoni, MD[b,e], Federico Lucherini, MSc [a,b], Nina Ajmone-Marsan, MD, PhD[f], Alberto Redaelli, PhD [a],
Gianfranco B. Fiore, PhD [a,b], Emiliano Votta, PhD [a], Carlo Antona, MD [b,e], and Riccardo Vismara, PhD [a,b]

aDepartment of Electronics, Information and Bioengineering, Politecnico di Milano, Milan, Italy; bForcardioLab – Fondazione per la Ricerca in Cardiochirurgia ONLUS, Milan, Italy; c3D and Computer Simulation Laboratory, IRCCS Policlinico San Donato, San Donato Milanese, Italy; dDivision of Cardiac Surgery, Department of Surgery, Università di Verona, Verona, Italy; eCardiovascular Surgery Department, ASST Fatebenefratelli Luigi Sacco University Hospital, Milan, Italy; fDepartment of Cardiology, Leiden University Medical Center, Leiden, The Netherlands

ABSTRACT

Background: Functional tricuspid regurgitation (FTR) treatment is challenging and most therapies targeting tricuspid valve (TV) annulus have shown limited durability with high rate of residual and recurrent regurgitation. In fact, right ventricular (RV) dilatation, which is another important determinant of FTR, remains unaddressed with these procedures. The aim of this study was to assess the effects of RV free wall approximation (FWA) toward the septal wall in an ex-vivo pulsatile model of FTR.

Methods: FWA was simulated in 15 porcine right hearts by approximating RV free wall at the anterior papillary muscle level toward the septal wall in three different directions.

Results: The treatment induced 19% decrease of regurgitation fraction with respect to pre-treatment and changes in TV morphology including reduction of TV tenting volume (up to 47%) and annulus size (up to 18%) as assessed via 3D computational reconstructions from echocardiographic volumetric data. The procedure success was significantly correlated ($R^2 = 0.91$) with TV annulus size ($p = .02$) when corrected for pre-treatment cardiac output.

Conclusions: As evaluated in the FTR experimental model, FWA significantly reduced TV regurgitation, leaflet tenting and annular dimension. Concomitant annular stabilization could improve the results as the pre-treatment dimension of TV annulus had an impact on FWA outcome.

Introduction

Normal tricuspid valve (TV) function results from the proper interaction of all TV components including the three leaflets, the annulus, the chordae tendineae and the papillary muscles (PMs). Right ventricular (RV) pressure and/or volume overload (i.e., by left heart-sided diseases) can induce chamber dilatation and tricuspid annulus (TA) enlargement. Both phenomena lead to leaflet malcoaptation and functional tricuspid regurgitation (FTR) due to leaflet displacement in the anteroposterior direction (by TA enlargement) and leaflet tethering (by RV dilatation).[1,2] FTR affects 1.6 million people in the USA and represents a serious public health problem.[3,4]

Currently, available FTR treatments target the TA and/or the TV leaflets directly[5,6], while RV dilatation and leaflet tethering remain unaddressed. When RV remains dilated high TV tenting volume was shown to be the predictor of residual FTR after tricuspid annuloplasty.[7] Moreover, RV dilatation can further progress over time, leading to FTR recurrence at follow-up.[5,8] Importantly, a re-operation for FTR was shown to be associated with high short- and long-term mortality and therefore should be prevented.[9]

Recently, the combination of annuloplasty and surgical treatment of the subvalvular apparatus was suggested to treat FTR[5,10], based on the clinical evidence obtained in the treatment of functional mitral regurgitation[11,12], which has similar mechanism and similar rate of recurrence.[13] However, so far only a small patient cohort study was reported with no FTR recurrence at 1-year follow-up after the combined treatment.[14] In the setting of FTR, a treatment which ensures a proper coaptation of the leaflets is challenging considering the specific anatomical position and mechanical properties of the RV and the complex anatomy of the TV apparatus.

The aim of this study was to quantify the effects of RV free wall approximation (FWA) on the severity of FTR and on TV morphology (with 3D anatomical reconstructions from echocardiographic volumetric data) using an ex-vivo pulsatile FTR model where the direction and the degree of FWA could be regulated.

Materials and methods

FTR experimental model

The pathological model exploited the tendency of right porcine heart to dilate spontaneously once under physiological pulmonary pressure in ex-vivo setup. The TA and RV dilation were observed, leading to TV malcoaptation, leaflets tenting and consequently the regurgitation.

FWA simulation in ex-vivo model

FWA was simulated in 15 porcine hearts obtained from a local abattoir by passing a surgical stitch through the RV. FWA was evaluated independently in three different anatomical directions corresponding to PMs position: (i) between anterior and posterior PM (A-P), (ii) between anterior and septal PM (A-S) and (iii) between anterior PM and the septal wall (central point between posterior and anterior PMs) (A-SW) (Figure 1a). In each tested direction the stitch was secured to a 3 cm diameter pad from the septal wall side, whereas from RV free wall side the stitch was fixed to a 3D-printed mechanical winch device (Figure 1b, 3 cm diameter), which allowed for tuning the intraventricular stitch length and to perform FWA. The degree of shortening of the intraventricular portion of the stitch was controlled by counting the revolutions of the winch. The device was intended to simulate possible surgical/interventional procedures' effects in a highly controllable manner.

Experimental setup and protocol

The porcine hearts featuring pathological FTR conditions were placed in a passive beating right heart platform[15,16] and were actuated by a pulsatile pump causing dynamic opening and closing of TV and pulmonary valve. The pulmonary artery was connected to a hydraulic circuit simulating pulmonary circulation impedance and featuring adjustable pulmonary resistance. The right atrium was connected to a preload reservoir. The working fluid was 0.9% NaCl at room temperature.

The pump was set to simulate the resting conditions (heart rate 60 beats/minute, pump stroke 70 mL, mean pulmonary artery pressure (PAP) 15 mmHg). After confirming the pathological state (pre-FWA) via fiberscope visualization, FWA of 30% and 60% (Figure 1c) in A-P, A-S, and A-SW directions were performed in a random order. The initial intraventricular stitch length for each direction of FWA was measured beforehand using echocardiography. In each state, hemodynamic (all 15 samples) and 3D echocardiographic (8 samples) acquisitions were performed using a transit-time flowmeter with a 1″ probe (HT110R, Transonic System, Inc., Ithaca, NY, USA), piezo-resistive pressure transducers (140PC series, Honeywell, Inc., Morristown, NJ, USA) and ECG-gated echocardiograph (IE33 with X7-2t probe, Philips, Eindhoven, The Netherlands).

Data processing

The following hemodynamic parameters were obtained upon averaging over 10 cardiac cycles:

- Cardiac output (CO), the time-averaged pulmonary flow,
- PAP,
- Change in tricuspid backflow fraction (ΔTBF), the absolute difference in tricuspid backflow fraction (ratio between backflow volume and forwardflow volume) between pre- and post-FWA,
- Change in pulmonary backflow fraction (ΔPBF), the absolute difference in pulmonary backflow fraction (ratio between backflow volume and forwardflow volume) between pre- and post-FWA,
- Mean diastolic pressure drop across the TV (Δp_t),
- Mean systolic pressure drop across the pulmonary valve (Δp_p).
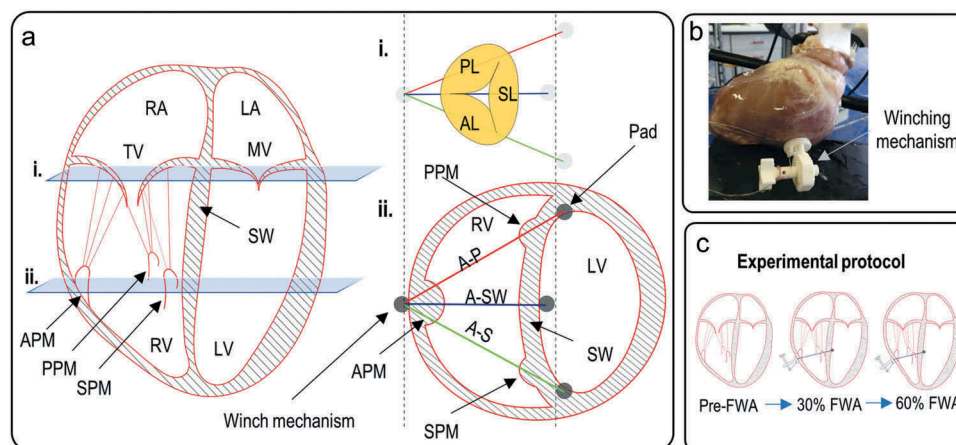
Figure 1. (a). Free wall approximation (FWA) experimental simulation technique: approximating stitch directions scheme in long axis and short axis (with view at i. valve and ii. papillary muscle level); (b). winching mechanism used to perform FWA in the experimental setup (c). experimental protocol: for each heart sample the data were registered in three conditions (pre-FWA, post-FWA at 30% and 60% degree of approximation) independently in 3 direction (for scheme clarity only A-SW direction is shown). AL = anterior leaflet, APM = anterior papillary muscle, A-P = anterior-posterior approximation direction, A-SW = anterior-septal wall approximation direction, A-S = anterior-septal approximation direction, MV = mitral valve, LA = left atrium, LV = left ventricle, PL = posterior leaflet, PPM = posterior papillary muscle, RA = right atrium, RV = right ventricle, SL = septal leaflet, SPM = septal papillary muscle, SW = septal wall, TV = tricuspid valve.
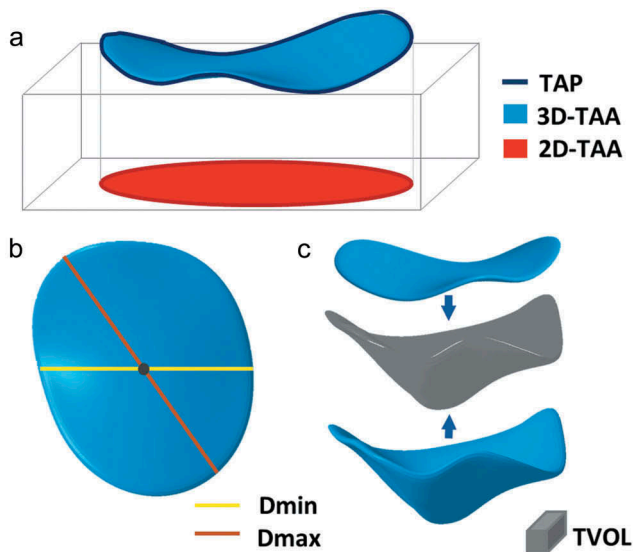
Figure 2. Tricuspid valve morphological parameters derived from 3D reconstructions of echocardiographic volumetric data. (a). 3D annular profile and its projection on best fit plane with depicted 3D (3D-TAA) and 2D annulus area (2D-TAA) and 3D annulus perimeter (TAP), (b). Annular profile and maximal (Dmax) and minimal diameter (Dmin) passing though the annulus centroid, (c). Tenting volume (TVOL) enclosed between 3D annular profile and leaflets surface.

ΔPBF, Δp_t, Δp_p were evaluated to assess if the FWA technique induced pulmonary valve malfunction or tricuspid valve stenosis.

Custom software developed in Matlab® (The Mathworks, Inc., Natick, MA, US) was used for the analysis of the morphology of the TV from the 3D echocardiographic acquisitions (8 samples). Specifically, 18 planes evenly rotated around the TV axis were automatically defined by interpolating the volumetric data. In-plane resolution was set isotropic and equal to the minimum spatial resolution of the original volumetric data. At the mid-systolic frame in each analyzed plane, two annular points were manually identified, and leaflets were manually traced.

Through principal component analysis of the cartesian coordinates of the annular points, their best-fit plane was identified, and coordinates were recomputed into a reference frame centered in the center of the annulus and having the z-axis orthogonal to the best-fit plane. Annular points were fitted though fourth order Fourier functions to obtain a continuous 3D annular profile.[17] The leaflet surface was defined as following: on each image plane, manually traced leaflet points were interpolated by a 2D cubic spline, which was resampled at 64 uniformly distributed points. The resulting 3D point-cloud (18×64) representing valve leaflets was fitted through a Loess function[18] to yield the continuous 3D leaflet surface.

The following morphological parameters were calculated from the 3D reconstructions (Figure 2):

- 3D TA area (3D-TAA), area enclosed within the 3D annular profile (Figure 2a),
- 2D TA area (2D-TAA), portion of area delimited by projection of the 3D annular profile on the best fit plane (Figure 2a),
- TA 3D perimeter (TAP), obtained from 3D annular profile (Figure 2a),
- TA maximal (Dmax) and minimal diameter (Dmin), the longest and shortest chord, respectively, connecting two annular points and crossing the centroid of the TA points (Figure 2b),
- Tenting volume (TVOL), the space enclosed between TV leaflets surface and 3D TA plane (Figure 2c).

Statistical assessment

All values were presented as mean ± standard deviation if data were normally distributed or as median (first interquartile; third interquartile) if not. The statistical significance of differences between pre- and post-FWA conditions was calculated using ANOVA for repeated measures or Friedman test when appropriate. Comparison between pre-FWA and each post-treatment condition was assessed by Dunnett's post hoc test, whereas the differences between post-treatment conditions were evaluated with a Bonferroni multiple comparison post hoc test. Dunn's multiple comparison test was used for non-parametric analysis. A p value < 0.05 was assumed as statistically significant. The predictors of post-treatment CO relative change ($[CO_{\text{pre-FWA}}-CO_{\text{post-FWA}}]/CO_{\text{pre-FWA}}*100\%$) were determined among baseline 3D-TAA, 2D-TAA, TAP, Dmax, Dmin, TVOL and CO by multiple linear regression using backward method with inclusion criteria $p < 0.1$. Highly correlated variables were removed from model to avoid collinearity ensuring variance inflation factor to be <2.5.

Results

TV function assessment before and after FWA

Figure 3 and the supplementary Video 1 show TV in mid-systole frame and in full cardiac cycle, respectively, before and after the treatment in fiberscope direct visualization (atrial view), Color Doppler, 3D echocardiography, computational reconstructions, and 3D-printed models.

Table 1 displays a summary of all hemodynamic and 3D reconstruction-derived echocardiographic parameters at pre- and post-FWA conditions for all three evaluated directions (A-P, A-S, A-SW) each one at two degrees of approximation (30%, 60%).

FWA induced overall increase of CO and PAP

Between pre- and post-FWA, CO increased significantly by 22–27% ($p \leq 0.003$) following 30% FWA and by 33–46% ($p \leq 0.001$) following 60% FWA, depending on the direction of approximation. CO changes corresponded to decrease in TV regurgitation (expressed quantitatively by ΔTBF) by 9–10% ($p \leq 0.09$) and by 14–19% ($p \leq 0.001$) as compared to pre-FWA after 30% and 60% approximation, respectively. The treatments did not induce neither significant ΔPBF nor increase in Δp_p and Δp_t, suggesting that FWA does neither alter pulmonic valve function nor induce tricuspid valve stenosis.
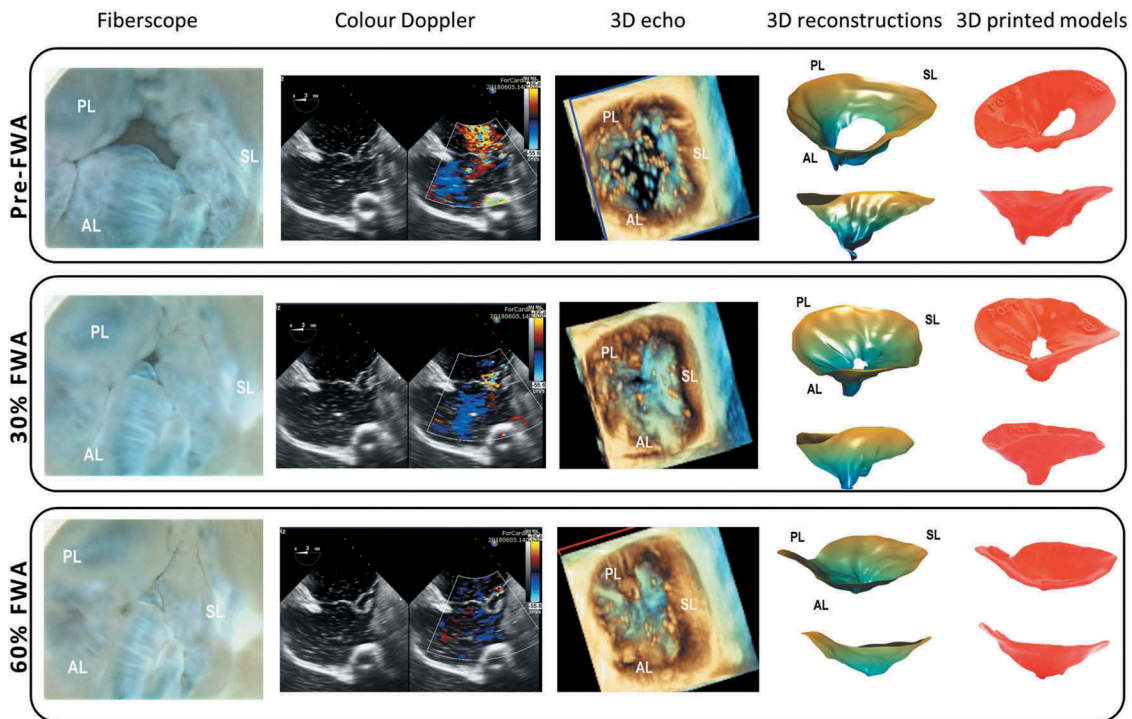
Figure 3. Representative tricuspid valve views from fiberscope (atrial view), Color Doppler, 3D echocardiography, 3D computational reconstructions and 3D-printed models at pre-FWA (first row), after 30% FWA (second row) and after 60% FWA (third row) in anteroposterior (A-P) direction. AP = anterior leaflet, FWA = free wall approximation, PL = posterior leaflet, SL = septal leaflet.

FWA induced also significant changes in TV morphology. Qualitatively, its effect on leaflets tenting and TA dimensions are evident from the TV 3D reconstructions (Figure 4). Quantitatively, TVOL was reduced by 31–39% ($p \leq 0.004$) and 44–47% ($p \leq 0.002$) following 30% and 60% FWA, respectively. Similarly, 3D-TAA, 2D-TAA, and TAP were reduced significantly in all tested directions after 60% FWA by maximum of 18%, 18% and 6%, respectively ($p < 0.05$).

Effect of approximation direction on TV hemodynamics and morphology

Local changes in TA orifice as well as regurgitation orifice dimension and morphology depended on the FWA direction as exemplified in Figure 5.

95% CI analysis (Figure 6) revealed quantitative insights on the effects of the specific directions on hemodynamics and TV morphology. Dependency on the direction of approximation was minor when 30% FWA was set, but increased following 60% of FWA. In the latter one, A-P and A-SW directions enabled greater increase of CO and decrease of 3D-TAA comparing to A-S direction. The trends in hemodynamics corresponded to the trend in 3D-TAA. Nevertheless, all directions provided similar reduction in TVOL in both tested levels of approximation.

Predictors of FWA outcome

Multiple regression analysis (Table 2) showed that post-FWA CO relative change was dependent on pre-FWA CO and Dmax in each evaluated direction at 60% degree of approximation ($p < 0.05$ for A-S direction and $p < 0.1$ for other directions). The estimated regression coefficients suggest that the treatment was most effective in smallest Dmax when corrected for pre-FWA CO. For instance, for the A-P direction, every increase of Dmax by 1 cm was associated with mean 56% reduction in relative post-FWA CO change. Correction for pre-FWA CO was necessary to account for baseline TV regurgitation and differences between samples related to the experimental model (ventricular compliance, pulmonary valve performance).

Discussion

In this study, TV regurgitation was addressed with a subvalvular approach in an ex-vivo FTR model. We systematically evaluated the impact of FWA, applied in three different directions, on right heart hemodynamics and TV morphology exploiting also 3D computational reconstructions. The outcomes showed that FWA was able to significantly reduce tricuspid regurgitation and TV morphological anomalies and the treatment success was dependent on and annulus dimensions when corrected for pre-treatment hemodynamics (related to the model).

Ex-vivo modeling

The study was performed using a pathological model which has been already exploited in steady[19,20] and pulsatile flow conditions.[16,21] This kind of modeling allows us to focus

Table 1. Overall hemodynamic and echocardiographic assessment of free wall approximation (FWA) in three directions (A-P, A-S, and A-SW) and two level of approximation (30% and 60% FWA). P-value columns correspond to comparison between 30% and 60% FWA. NS = not significant according to ANOVA for repeated measures. A-P = anterior-posterior FWA direction, A-S = anterior-septal FWA direction, A-SW = anterior-septal wall FWA direction, CO = cardiac output, PAP = mean pulmonary artery pressure, ΔTBF = change in tricuspid backflow fraction, ΔPBF = change in pulmonary backflow fraction, Δp_t = mean diastolic pressure drop across tricuspid valve, Δp_p = mean systolic pressure drop across pulmonary valve, TVOL = tenting volume, TAP = tricuspid annulus perimeter, 3D-TAA = 3-dimentional tricuspid annulus area, 2D-TAA = tricuspid annulus area projected on 2D plane, Dmax = maximal tricuspid annulus diameter, Dmin = minimal tricuspid annulus diameter.

Parameter	Pre-FWA	Post-FWA								
		A-P direction			A-S direction			A-SW direction		
		30%	60%	p-value	30%	60%	p-value	30%	60%	p-value
Hemodynamics (15 samples)										
CO, L/min	2.2 ± 0.6	2.7 ± 0.7 (p = 0.003)	3.1 ± 0.8 (p < 0.001)	<0.001	2.7 ± 0.7 (p = 0.002)	2.9 ± 0.7 (p < 0.001)	0.01	2.8 ± 0.7 (p < 0.001)	3.2 ± 0.7 (p < 0.001)	<0.001
PAP, mmHg	16.0 ± 4.0	17.0 ± 3.8 (p = 0.7)	18.7 ± 3.9 (p = 0.04)	0.02	17.1 ± 4.8 (p = 0.6)	18.5 ± 5.1 (p = 0.09)	0.3	17.3 ± 4.0 (p = 0.2)	18.7 ± 4.1 (p = 0.02)	0.002
ΔTBF, %	0	9(3; 14) (p = 0.03)	18(10; 20) (p < 0.001)	0.004	9(3; 15) (p = 0.09)	14(7; 19) (p < 0.001)	0.1	10(3; 15) (p = 0.03)	19(15; 21) (p < 0.001)	0.009
ΔPBF, %	0	1(−1; 2) (NS)	0(−1; 3) (NS)	NS	0(−2; 2) (NS)	1(−3; 2) (NS)	NS	1(−1;2) (NS)	2(−1;2) (NS)	NS
Δp_t, mmHg	1.2 ± 0.7	1.0 ± 0.8 (NS)	1.0 ± 0.8 (NS)	NS	0.8 ± 0.4 (NS)	1.0 ± .8 (NS)	NS	1.6 ± 1.0 (NS)	1.4 ± 0.9 (NS)	NS
Δp_p, mmHg	5.1 ± 1.5	6.0 ± 1.5 (NS)	5.6 ± 2.2 (NS)	NS	6.1 ± 2.3 (NS)	6.4 ± 2.5 (NS)	NS	6.3 ± 1.9 (NS)	7.3 ± 2.4 (NS)	NS
Tricuspid valve morphology derived from 3D reconstructions of volumetric echocardiography (8 samples)										
TVOL, mL	10.6 ± 3.1	7.3 ± 3.5 (p = 0.004)	5.8 ± 2.9 (p < 0.001)	NS	6.5 ± 2.2 (p < 0.001)	5.6 ± 2.3 (p = 0.001)	NS	6.8 ± 2.7 (p = 0.003)	5.9 ± 2.2 (p = 0.002)	NS
3D-TAA, cm^2	21.3 ± 2.7	19.0 ± 2.8 (p = 0.04)	17.5 ± 2.5 (p = 0.007)	0.02	18.7 ± 3.0 (0.002)	18.7 ± 3.0 (0.003)	1	18.9 ± 2.3 (p < 0.001)	18.0 ± 2.0 (p < 0.001)	0.3
2D-TAA, cm^2	20.2 ± 2.8	17.9 ± 2.7 (p = 0.02)	16.5 ± 2.4 (p = 0.008)	0.04	18.0 ± 3.2 (p = 0.01)	18.0 ± 3.2 (p = 0.006)	1	17.6 ± 2.4 (p = 0.003)	16.7 ± 1.9 (p = 0.001)	0.4
TAP, cm	16.1 ± 1.1	15.7 ± 1.2 (p = 0.04)	15.1 ± 1.0 (p = 0.007)	0.04	15.6 ± 1.4 (p = 0.006)	15.6 ± 1.2 (p = 0.006)	1	15.8 ± 1.0 (p = 0.001)	15.4 ± 0.9 (p < 0.001)	0.03
Dmax, cm	5.5 ± 0.4	5.3 ± 0.4 (p = 0.2)	5.0 ± 0.4 (p = 0.08)	NS	5.2 ± 0.6 (p = 0.2)	5.2 ± 0.5 (p = 0.1)	NS	5.3 ± 0.5 (p = 0.07)	5.1 ± 0.4 (p = 0.006)	NS
Dmin, cm	4.6 ± 0.4	4.3 ± 0.4 (p = 0.03)	4.1 ± 0.5 (p = 0.04)	NS	4.4 ± 0.5 (p = 0.5)	4.3 ± 0.5 (p = 0.2)	NS	4.1 ± 0.4 (p = 0.04)	4.0 ± 0.4 (p = 0.02)	NS
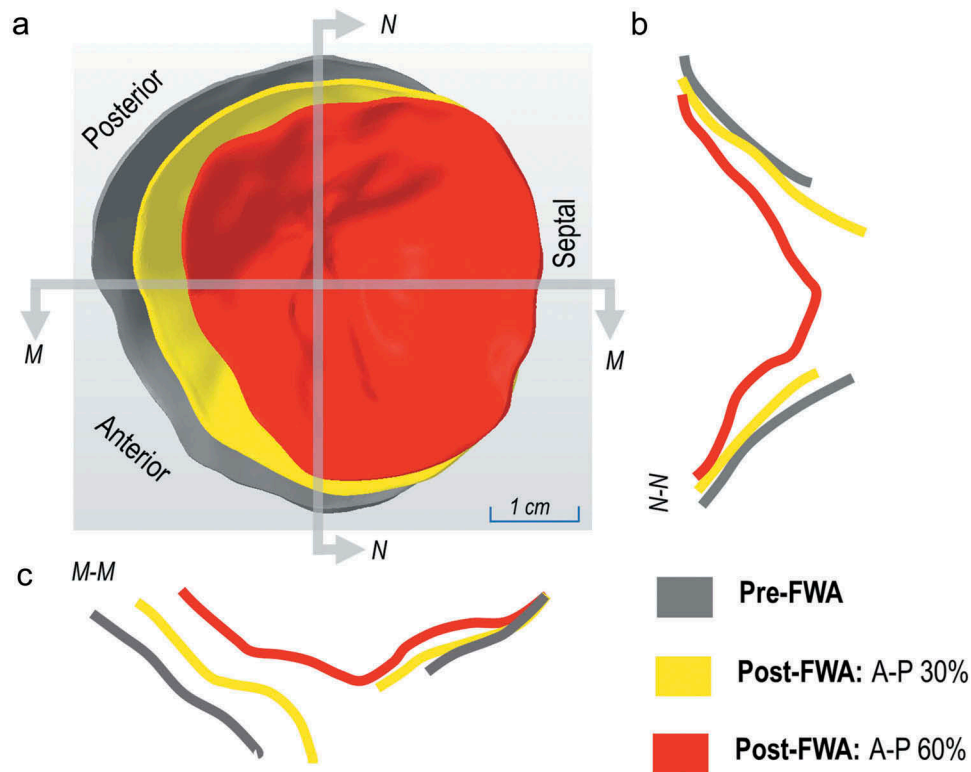
Figure 4. The influence of the free wall approximation (FWA) on annulus dimensions and leaflet tenting obtained from reconstructed models of a representative heart sample in pre- and post-FWA conditions in anteroposterior (A-P) direction. (a). Atrial view of tricuspid valve annulus and leaflets. (b). Leaflet profile in anteroposterior cross-section and (c). Leaflet profile in septo-lateral cross-section. The drawing was derived by aligning the three 3D reconstructions at the septal portion of the annulus (the most constrained part of the annulus, which displacement due to FWA was assumed minimal).
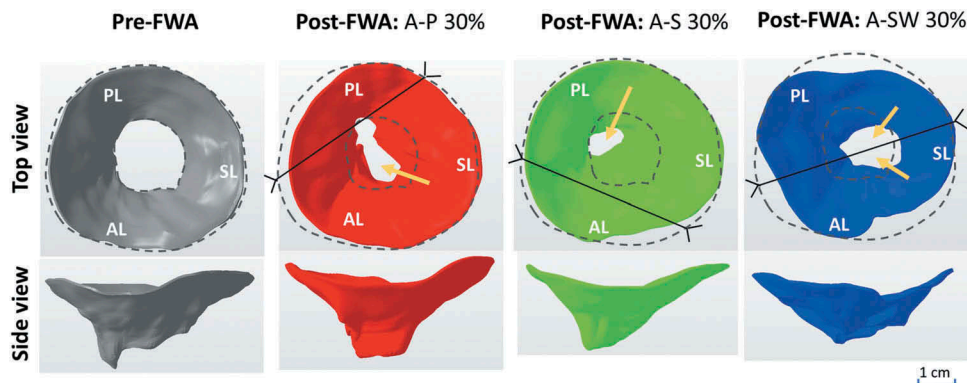
Figure 5. Example of tricuspid valve 3D reconstructions in baseline conditions (left panel) and post free wall approximation (FWA) by 30% in three evaluated directions (A-P: red, A-S: green, A-SW: blue) in a representative sample. Gray dashed lines indicate the annulus orifice and regurgitation orifice in pre-FWA conditions. Solid black lines indicate the directions of the approximation. Yellow arrows indicate the changes in regurgitation orifice related to local changes in valve tenting following specific directions of approximation.

specifically on the mechanistic effects of the treatment on hemodynamics and valve morphology. The type of RV dilation we obtained can be compared to isolated RV dilation (due to the lack of left ventricle) which clinically was associated with lateral displacement of all three PMs (and apical displacement of anterior PM) which leads to the most severe FTR form when compared with biventricular dilation or isolated left-ventricular dilation.[22]

The overall trends in terms of regurgitation reduction and TV geometrical reconfiguration following the FWA obtained in the present study were in agreement with the only

preliminary experimental study available in the literature where FTR was addressed by RV papillary muscle approximation.[20] Of note, Yamauchi et al. adopted steady flow conditions, while in the present work pulsatile flow conditions allowed us to reproduce more realistic scenarios, to account for transient states (TV closing and opening motion) and to exclude the risk for pulmonic valve malfunction (stenosis or regurgitation) and TV stenosis which could possibly be induced by FWA.[20] Also, Yamauchi et al. 2D ultrasound examinations were performed, while we exploited 3D ultrasound to yield more exhaustive TV 3D

Approximation		Means difference (95% CI)	p-value
CO, L/min			
60%	A-P	0.9 (0.4, 1.3)	<0.001
	A-S	0.7 (0.3, 1.1)	<0.001
	A-SW	1.0 (0.7, 1.3)	<0.001
30%	A-P	0.5 (0.2, 0.9)	0.003
	A-S	0.5 (0.2, 0.8)	0.002
	A-SW	0.5 (0.3, 0.8)	<0.001
TVOL, mL			
60%	A-P	-4.9 (-7.2, -2.6)	<0.001
	A-S	-5.0 (-7.5, -2.5)	0.001
	A-SW	-4.8 (-7.3, -2.2)	0.002
30%	A-P	-3.4 (-5.4, -1.3)	0.004
	A-S	-4.2 (-6.1, -2.2)	<0.001
	A-SW	-3.9 (-6.1, -1.7)	0.003
3D-TAA, cm^2			
60%	A-P	-3.8 (-6.4, -1.2)	0.007
	A-S	-2.6 (-4.1, -1.1)	0.003
	A-SW	-3.4 (-4.9, -1.9)	<0.001
30%	A-P	-2.4 (-4.6, -0.1)	0.04
	A-S	-2.7 (-4.1, -1.3)	0.002
	A-SW	-2.5 (-3.7, -1.3)	<0.001
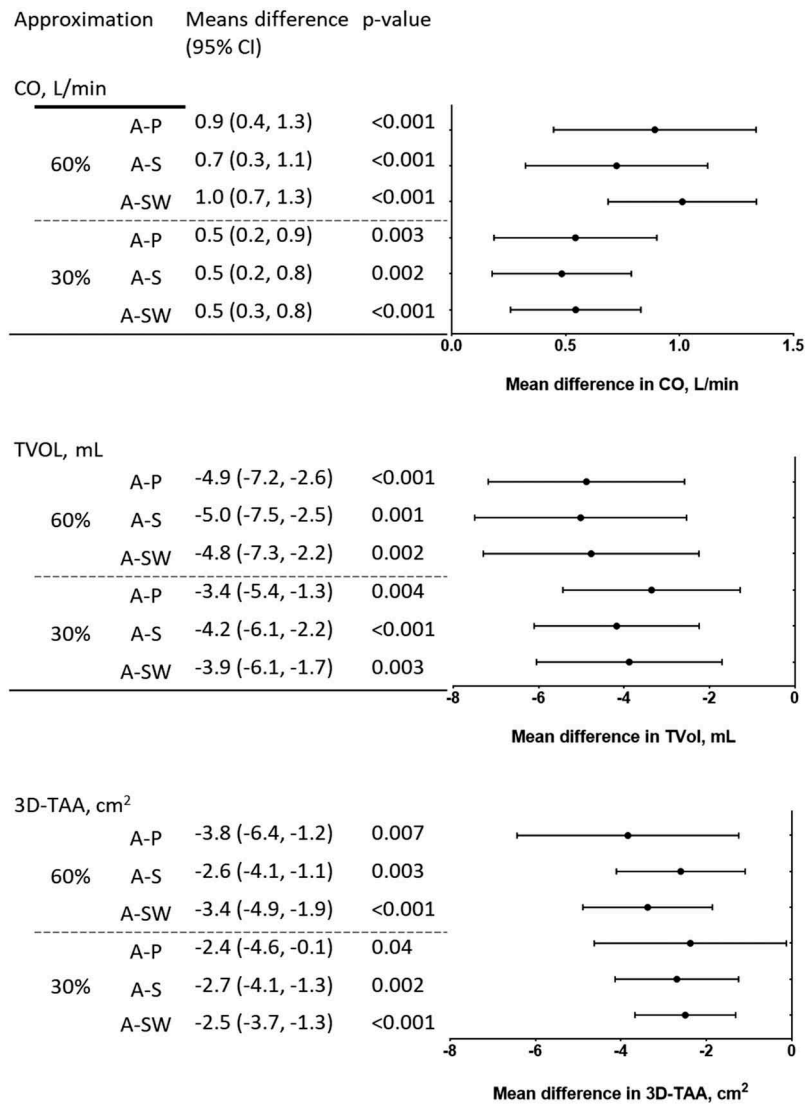
Figure 6. Mean differences, 95% confidence intervals (CI) and p-values between pre-FWA (free wall approximation) and post-FWA conditions for cardiac output (CO), tenting volume (TVOL) and 3D tricuspid annulus area (3D-TAA) at 30% and 60% degree of FWA for each direction of approximation (A-P, A-S, A-SW).

Table 2. Predictors of post-FWA (papillary muscle approximation) cardiac output (CO) relative change from multiple regression model for each direction of approximation (A-P, A-S, A-SW) at 60% of approximation. For each predictor following data is provided: regression coefficient (95% confidence intervals), significance value.

| Direction	Post-FWA CO change (mean±std)	Predictors		Adjusted R^2
		CO (pre-FWA), L/min	Dmax (pre-FWA), cm	
A-P 60%	+51 ± 58%	−0.72 (95% CI: −1.10, −0.34), $p = 0.003$	−0.56 (95% CI: −1.22, 0.1), $p = 0.08$	0.72
A-S 60%	+48 ± 40%	−0.58 (95% CI: −0.79, −0.37), $p = 0.001$	−0.59 (95% CI: −1.0, −0.18), $p = 0.02$	0.91
A-SW 60%	+54 ± 51%	−0.61 (95% CI: −1.02, −0.19), $p = 0.01$	−0.66 (95% CI: −1.46, 0.15), $p = −0.09$	0.66

reconstructions and descriptors of the pathology accounting for the complex 3D TV shape.[20]

Impact of the direction of the approximation on hemodynamics and TV morphology

Gross changes in hemodynamics and TV morphology were improving with increasing degree of FWA. They were comparable in all evaluated directions regardless if the direction of approximation targeted the PMs located at the septal wall directly (A-P and A-S directions) or not (A-SW direction). Nonetheless, considering the biomechanics and TV apparatus anatomy, different local tenting in between each leaflet pair can be expected (Figure 7) depending on the FWA direction as depicted on exemplary TV reconstructions in Figure 5. Hence, A-P direction should favor reaching higher positions of free leaflet edges at the postero-septal commissure. On the contrary, A-S approximation could reduce up to higher degree the tenting between anterior and septal leaflet, whereas A-SW direction should improve the tenting between all 3 leaflet pairs in the same way. Therefore, A-S and A-P directions
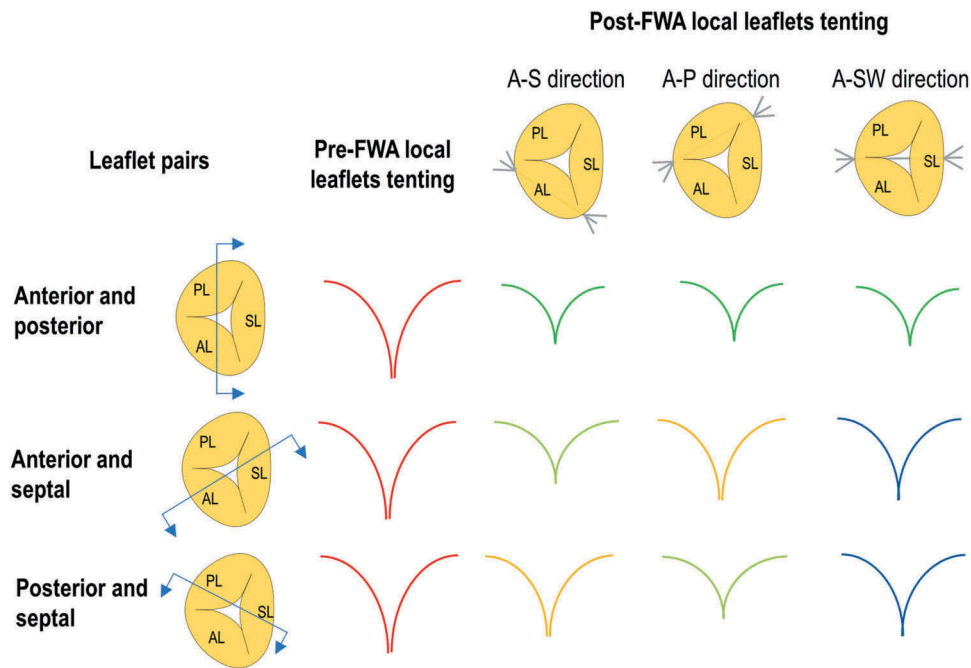
Figure 7. Expected change in local tenting in between leaflets pair following the approximation in A-P, A-S and A-SW direction. The severity of local tenting was color-coded in the following order: red, orange, blue, green corresponding to the highest and lowest tenting.

could be more favorable in specific cases, e.g., in coaptation defects only in between septal and anterior or septal and posterior leaflet, respectively. These observations require additional deeper quantitative assessment to unambiguously demonstrate the influence of the treatment direction on TV tenting.

Effects of the treatment and related benefits

The impact of FWA on TV morphology can have a fourfold effect. First, by displacing the PMs, FWA reduced TV tenting, reduced restricted leaflet motion and thus enabled coaptation at higher points. Second, FWA decreased TA size. These two effects contributed to reducing TV regurgitation. Third, it can be speculated that by relieving leaflet tethering FWA could have a positive impact on leaflet mechanical stress distribution[23] and chordae forces reduction[24] preventing long-term structural remodeling. Fourth, it is reasonable to presume that FWA reduces the chances of recurrent RV dilatation, owing to the mechanical constraint between the septal region and the free wall. These two further potential effects could enhance the long-term durability of TV therapy.

Annulus size influence

In our study, FWA success was dependent on the baseline TA size, which implies that FWA could be less effective in the presence of severely dilated annulus. Indeed, FWA does not address the annulus directly. This finding is opposed to the conclusions of Yamauchi et al. study[20] which suggested that subvalvular approach repairs better repairs FTR with respect to TV annuloplasty, as the authors did not consider TA baseline dimension in their analysis. Moreover, in our study, the baseline TVOL did not influence significantly subvalvular-level treatment outcomes, while clinically

it was a significant predictor of residual regurgitation and pathology recurrence following annuloplasty.[7,8] This evidence suggests that FWA could be a promising approach in the case of highly dilated right ventricles with preprocedural high tenting and could be an alternative to surgical leaflet augmentation technique.[25]

The concomitant approach directly addressing both FTR contributors, PM displacement (by subvalvular approach) and TA dilatation (by, e.g., annuloplasty), could be the most effective in reducing regurgitation and TV morphological anomalies with a potential for therapy durability improvement. While in case of isolated TA enlargement, induced by, e.g., atrial fibrillation[26], annular-level treatment could be sufficient.

Clinical translation

The results encourage translation of the concept into an interventional approach. The transthoracic minimally invasive access to the RV seems feasible based on the available literature[27] and a prototype of an implantable device together with its delivery tool is under development in our laboratory. However, its assessment is beyond the scope of this paper.

Limitations

The study carries intrinsic limitations of ex-vivo beating heart model. This modeling setup allows for quantification of acute post-treatment hemodynamic and morphological alterations only. The model lacks some of the clinically present phenomena (interaction with left ventricle, breathing influence on TV competence, feedback mechanisms, mechanobiological remodeling) and coexisting comorbidities (e.g., metabolic abnormalities). On the other hand, it allowed us to specifically focus on the mechanistic effects of the treatment. RV filling by the pump prevented

us from evaluating the influence of the FWA on RV diastolic function. For all these aspects, results need to be further assessed in-vivo.

In this work, we used a laboratory device allowing us to simulate the possible procedure effects with tight control over treatment configurations (different directions and degrees of approximation).

Conclusions

Addressing FTR via subvalvular approach reduced TV tenting, TA dimension and TV regurgitation similarly in all evaluated approximation directions in an ex-vivo model, which can be considered promising for future clinical application. The FWA procedure outcomes were found dependent on baseline cardiac output and TA size, suggesting that concomitant treatment at the valvular and subvalvular levels could provide better results.

ORCID

Michal Jaworek http://orcid.org/0000-0002-1484-8913
Omar A. Pappalardo http://orcid.org/0000-0003-0682-9349
Matteo Selmi http://orcid.org/0000-0002-6928-4588
Guido Gelpi http://orcid.org/0000-0002-2269-2111
Federico Lucherini http://orcid.org/0000-0003-4842-5000
Alberto Redaelli http://orcid.org/0000-0002-9020-2188
Gianfranco B. Fiore http://orcid.org/0000-0002-8988-8311
Emiliano Votta http://orcid.org/0000-0001-7115-0151
Carlo Antona http://orcid.org/0000-0002-9003-0240
Riccardo Vismara http://orcid.org/0000-0003-2646-1633

Funding

Disclosure statement

No potential conflict of interest was reported by the authors.

References

1. Spinner EM, Shannon P, Buice D, et al. In vitro characterization of the mechanisms responsible for functional tricuspid regurgitation. *Circulation*. 2011;124(8):920–929. doi:10.1161/CIRCULATIONAHA.110.003897.
2. Mascherbauer J, Maurer G. The forgotten valve: lessons to be learned in tricuspid regurgitation. *Eur Heart J*. 2010;31 (23):2841–2843. doi:10.1093/eurheartj/ehq303.
3. Taramasso M, Pozzoli A, Guidotti A, et al. Percutaneous tricuspid valve therapies: the new frontier. *Eur Heart J*. 2017;38(9):639–647. doi:10.1093/eurheartj/ehv766.
4. Topilsky Y, Maltais S, Medina Inojosa J, et al. Burden of tricuspid regurgitation in patients diagnosed in the community setting. *JACC Cardiovasc Imaging*. 2019;12(3):433–442. doi:10.1016/j.jcmg.2018.06.014.
5. Navia JL, Nowicki ER, Blackstone EH, et al. Surgical management of secondary tricuspid valve regurgitation: annulus, commissure, or leaflet procedure? *J Thorac Cardiovasc Surg*. 2010;139(6):1473–1482.e5. doi:10.1016/j.jtcvs.2010.02.046.
6. Rodés-Cabau J, Hahn RT, Latib A, et al. Transcatheter therapies for treating tricuspid regurgitation. *J Am Coll Cardiol*. 2016;67 (15):1829–1845. doi:10.1016/j.jacc.2016.01.063.
7. Min SY, Song JM, Kim JH, et al. Geometric changes after tricuspid annuloplasty and predictors of residual tricuspid regurgitation: a real-time three-dimensional echocardiography study. *Eur Heart J*. 2010;31(23):2871–2880. doi:10.1093/eurheartj/ehq227.
8. Fukuda S, Gillinov AM, McCarthy PM, et al. Determinants of recurrent or residual functional tricuspid regurgitation after tricuspid annuloplasty. *Circulation*. 2006;114(1 Suppl):I582–7. doi:10.1161/CIRCULATIONAHA.105.001305.
9. Bernal JM, Morales D, Revuelta C, Llorca J, Gutiérrez-Morlote J, Revuelta JM. Reoperations after tricuspid valve repair. *J Thorac Cardiovasc Surg*. 2005;130(2):498–503. doi:10.1016/j.jtcvs.2004.12.044.
10. Ooka T, Matsui Y. Tricuspid valve surgery based on the mechanisms of functional tricuspid regurgitation. *Ann Thorac Cardiovasc Surg*. 2012;18(4):293–296. doi:10.5761/atcs.ed.12.01935.
11. Nappi F, Lusini M, Spadaccio C, et al. Papillary muscle approximation versus restrictive annuloplasty alone for severe ischemic mitral regurgitation. *J Am Coll Cardiol*. 2016;67(20):2334–2346. doi:10.1016/j.jacc.2016.03.478.
12. Harmel EK, Reichenspurner H, Girdauskas E. Subannular reconstruction in secondary mitral regurgitation: a meta-analysis. *Heart*. 2018;104(21):1783–1790. doi:10.1136/heartjnl-2017-312277.
13. Bouma W, van der Horst ICC, Wijdh-den Hamer IJ, et al. Chronic ischaemic mitral regurgitation. Current treatment results and new mechanism-based surgical approaches□. *Eur J Cardiothoracic Surg*. 2010;37(1):170–185. doi:10.1016/j.ejcts.2009.07.008.
14. Ouda A, Matschke K, Ghazy T, et al. Right ventricular reduction for repair of functional tricuspid valve regurgitation: one-year follow up. *J Heart Valve Dis*. 2013;22(5):754–761. http://www.ncbi.nlm.nih.gov/pubmed/24383394. Accessed July 19, 2016.
15. Jaworek M, Piola M, Lucherini F, et al. Functional tricuspid regurgitation model in a beating heart platform. *ASAIO J*. 2017;63(4):438–444. doi:10.1097/MAT.0000000000000510.
16. Vismara R, Gelpi G, Prabhu S, et al. Transcatheter edge-to-edge treatment of functional tricuspid regurgitation in an ex vivo pulsatile heart model. *J Am Coll Cardiol*. 2016;68(10):1024–1033. doi:10.1016/j.jacc.2016.06.022.
17. Sturla F, Onorati F, Puppini G, et al. Dynamic and quantitative evaluation of degenerative mitral valve disease: a dedicated framework based on cardiac magnetic resonance imaging. *J Thorac Dis*. 2017;9(Suppl 4):S225–S238. doi:10.21037/jtd.2017.03.84.
18. Cleveland WS. Robust locally weighted regression and smoothing scatterplots. *J Am Stat Assoc*. 1979;74(368):829–836. doi:10.1080/01621459.1979.10481038.
19. Maisano F, Taramasso M, Guidotti A, et al. Simulation of functional tricuspid regurgitation using an isolated porcine heart model. *J Heart Valve Dis*. 2011;20(6):657–663. http://www.ncbi.nlm.nih.gov/pubmed/22655496.
20. Yamauchi H, Vasilyev NV, Marx GR, et al. Right ventricular papillary muscle approximation as a novel technique of valve repair for functional tricuspid regurgitation in an ex vivo porcine model. *J Thorac Cardiovasc Surg*. 2012;144(1):235–242. doi:10.1016/j.jtcvs.2012.01.028.
21. Jaworek M, Gelpi G, Romagnoni C, et al. Long-arm clip for transcatheter edge-to-edge treatment of mitral and tricuspid regurgitation – ex-vivo beating heart study. *Struct Heart*. 2019;3 (3):211–219. doi:10.1080/24748706.2019.1590666.
22. Spinner EM, Lerakis S, Higginson J, et al. Correlates of tricuspid regurgitation as determined by 3D echocardiography: pulmonary arterial pressure, ventricle geometry, annular dilatation and papillary muscle displacement. *Circ Cardiovasc Imaging*. 2011;5 (1):43–50. doi:10.1161/CIRCIMAGING.111.965707.
23. Chandran KB, Kim H. Computational mitral valve evaluation and potential clinical applications. *Ann Biomed Eng*. 2015;43 (6):1348–1362. doi:10.1007/s10439-014-1094-5.

24. Troxler LG, Spinner EM, Yoganathan AP. Measurement of strut chordal forces of the tricuspid valve using miniature C ring transducers. *J Biomech.* 2012;45(6):1084–1091. doi:10.1016/j.jbiomech.2011.12.004.

25. Dreyfus GD, Raja SG, John Chan KM. Tricuspid leaflet augmentation to address severe tethering in functional tricuspid regurgitation. *Eur J Cardiothoracic Surg.* 2008;34(4):908–910. doi:10.1016/j.ejcts.2008.07.006.

26. Topilsky Y, Khanna A, Le Tourneau T, et al. Clinical context and mechanism of functional tricuspid regurgitation in patients with and without pulmonary hypertension. *Circ Cardiovasc Imaging.* 2012;5(3):314–323. doi:10.1161/CIRCIMAGING.111.967919.

27. Halabi M, Ratnayaka K, Faranesh AZ, et al. Transthoracic delivery of large devices into the left ventricle through the right ventricle and interventricular septum: preclinical feasibility. *J Cardiovasc Magn Reson.* 2013;15(1):10. doi:10.1186/1532-429X-15-10.